PCCP

Accepted Manuscript

ROYAL SOCIETY OF CHEMISTRY

www.rsc.org/pccp

Conjugated Polymer P3HT /Au Hybrid Nanostructure for Enhancing Photocatalytic Activity

Bikash Jana, Santanu Bhattacharyya, Amitava Patra*

Department of Materials Science, Indian Association for the Cultivation of Science,

Kolkata 700 032, India

*Author to whom correspondence should be addressed. Electronic mail: msap@iacs.res.in. Telephone: (91)-33-2473-4971. Fax: (91)-33-2473-2805.

Abstract

Metal-semiconductor nanostructures have been the subject of great interest, mainly due to their interesting optical properties and their potential applications in light harvesting, photocatalysis and photovoltaic devices. Here, we have designed raspberry type organic-inorganic hybrid nanostructures of Poly-3-hexylthiophene (P3HT) -Au nanoparticle (NP) composite by simple solution based synthetic method. The electronic interaction of semiconducting P3HT polymer nanoparticle with Au nanoparticle exhibits bathochromic shift of absorption band and significant photoluminescence quenching of P3HT nanoparticles in this organic-inorganic hybrid system. The photocatalytic activity of this raspberry type hybrid nanostructure is demonstrated under the visible light irradiation and the degradation efficiency is found to be 90.6%. Such organic-inorganic hybrid nanostructures made of semiconducting polymer and plasmonic nanoparticle could pave the way for designing new optical based materials for the applications in photocatalytic, and light harvesting system.

TOC:

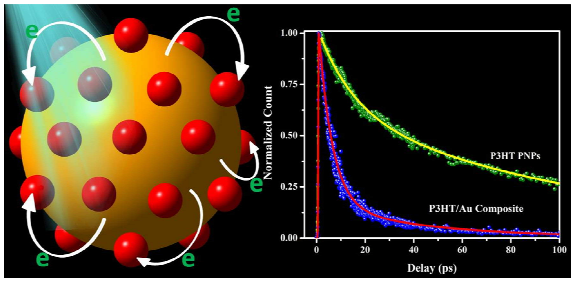

Highlights: Organic-inorganic hybrid nanostructures for designing new optical based materials for efficient photocatalysis

Introduction:

The investigation of hybrid nanostructures has attracted a great deal of interest, because of their potential applications in light emitting diodes (LEDs), optoelectronics, photovoltaics (PV), photocatalysis and others.[1-6] To date, major emphasis has been given on the interactions in organic/inorganic hybrid system to improve charge separation by suppressing charge recombination. The tuning of electronic energy level alignments by manipulating size and shape promote both charge separation and the energy transfer between organic and inorganic nanoparticles upon photoexcitation.[7, 8] Free charge carrier dynamics at organic/inorganic interface plays a crucial role in photovoltaic and photocatalysis properties.[7] Thus, the fundamental studies of charge carrier generation, electron transfer, and energy transfer in organic/inorganic hybrid nanostructures is very important because it dictates the overall efficiencies of the devices. For example, hyper-efficient energy transfer from conjugated polymer to gold NPs have been described by Fan et al.[9] Warner et al. enlisted the energy transfer phenomenon occurring from MEH-PPV to PbS nanocrystals.[10] Where, Greenham et al. reported the charge separation and transport in conjugated-polymer/semiconductor-nanocrystal composites.[11] Extensive studies have been persuaded to understand the electron transfer/ charge transfer dynamics in inorganic/ organic hybrid systems.[12-19] Hybrid system composed of π-conjugated polymers and inorganic nanoparticles (NPs) remains frontier area of research,[20-22] because organic part possesses significantly large absorption cross section due to delocalized π-electron transition from ground state (S_0) to excited state (S_n) and inorganic part exhibits unique optical properties due to quantum confinement.

Unprecedented electrical and optical properties of hybrid nano-materials are found which are much different from their individual counterparts.[7, 18, 20] The distinct properties of the polymer-metal nanoparticle hybrid system are due to exciton-plasmon interaction which

are different from its individual counterpart[23] and this hybrid system exhibits enhanced absorption cross sections, increase radiative rates and exciton-plasmon energy transfer due to weak coupling regime.[24] Basically, π-conjugated polymers are inherently multichromophoric systems, in which every monomeric unit is composed of π-electrons over a significant chain length.[25] On the other hand, surface plasmon resonance band originates from inorganic metal nanoparticle due to coherent excitation of free conduction electrons on the metal nanoparticle surface.[26, 27] The energy transfer /charge separation occurs due to the interaction between excited state of conjugated organic part and plasmonic band of metal nanoparticles upon photo-excitation. It is reported the surface plasmon of metal NPs influences the charge transfer process between excited metal NPs and conjugated polymer.[23]

In spite of optoelectronic applications of organic/inorganic hybrid systems, this hybrid system may be applied for photocatalysis because of the efficient photo-induced energy/ charge transfer dynamics. Herein, a new type of metal-semiconductor polymer nanostructure has been developed for efficient photo catalyst. We have designed raspberry type hybrid nanostructures by using negatively charged citrate capped Au NPs with positively charged surface functionalized regio-random P3HT polymer nanoparticles (PNPs). These regio-random P3HT and Au NPs are chosen because of HOMO-LUMO position of regio-random P3HT matches with the work function of Au NPs. Where, HOMO level of regio-random P3HT is around -5.5 eV with a band gap of 2.3 eV[28] and the work function of Au NPs is at -5.1 eV.[29] Thus, after light irradiation on the hybrid conjugate, Frenkel excitons (electrons and holes) are generated inside P3HT PNPs and dissociates at the organic/inorganic interface.[16] A charge separation between electrons and holes occurs during the transfer the photoexcited electrons of P3HT PNPs to Au NPs. Here, we investigate the ultrafast photo-physical processes of conjugated polymer P3HT NP-Au NP composite system by using picosecond TCSPC measurement, followed by ultrafast femtosecond fluorescence upconversion

technique. Furthermore, efficient photo-catalytic degradation of methylene blue (MB) under visible light illumination is studied due to photoinduced electron transfer process from P3HT to Au NP. This unprecedented photocatalytic activity of semiconducting polymer-plasmonic nanomaterials hybrid systems may open up a new aspect of applications for designing photovoltaic devices, optoelectronic devices as well as hybrid solar cells.

Results and discussion:

Polymer nanoparticles (PNPs) were prepared by re-precipitation technique,[30-32] P3HT in THF was rapidly injected into polar aqueous medium under vigorous stirring conditions. As a result, hydrophobic P3HT polymer molecules immediately coiled up to form P3HT PNPs to avoid contact with polar aqueous environment. In this procedure, PNPs are negatively charged (measured Zeta potential value in water is -18.7 mV) due to surface defects. For surface charge modification, we have taken a mixture of P3HT and hexadecylamine (HDA), in THF and then the mixed solution was re-precipitated in water. Finally positive surface charged P3HT PNPs (measured Zeta potential value +12.3 mV) were obtained. HDA has long hydrophobic saturated aliphatic chain with an amine group. This aliphatic long chain will go inside the core of polymer NP leaving the NH_2 group at the surface of the PNP. Figure 1A shows the TEM image of P3HT PNPs. The measured average particle diameter of positively charged PNPs is ~100 nm (± 10 nm). Further, Au NPs were prepared through the simple reduction method of aqueous solution of $HAuCl_4$ by freshly prepared ice cold aqueous solution of $NaBH_4$ in presence of trisodium citrate (used as capping ligand) under vigorously stirring condition.[33, 34] The measured average particle diameter of citrate capped Au NPs (depicted in fig. 1B) is 5.5 ± 0.2 nm. The measured zeta potential data is -22.4 mV for citrate capped Au NPs. After gradual addition of Au nanoparticle on surface modified P3HT PNPs solution, a hybrid conjugate system is easily formed (Depicted in Figure 1C and 1D) by electro-statically attached on positive charged

P3HT PNPs and the calculated zeta potential value is + 9.2 mV, confirms the raspberry structure formation by electrostatic interaction between metal and organic nanoparticles.

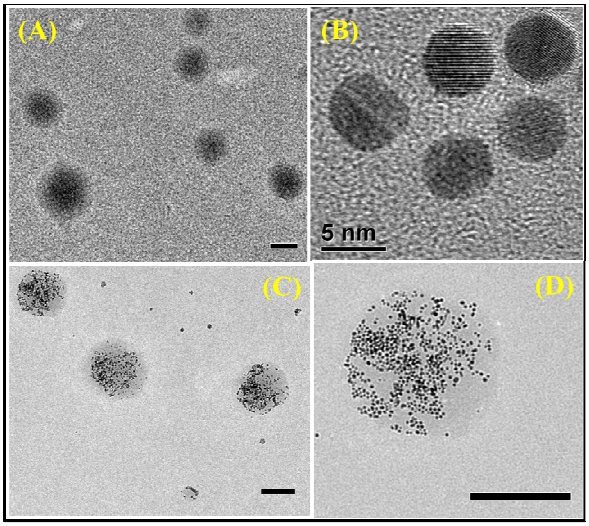

Fig. 1: TEM images of pure P3HT PNPs (A), Au NPs (B) and P3HT PNPs/ Au NPs composite (C), (D) (Scale bar for (A), (C) and (D) is 100 nm)

Steady state spectroscopic study has been undertaken to obtain more detail information about the intermolecular interactions of P3HT in nanoparticle form. In THF solution of P3HT, a broad absorption band with peak maxima at ~ 427 nm is due to strongly allowed π-π^* transition of conjugated back bone.[30] A red shifted absorption maximum at 440 nm (Shown in Fig. S1) is observed after nanoparticle formation which is consistent with previous result.[30] Wang et al. reported that the red shifting of absorption occurs due to relatively relaxed and ordered conformations.[35] THF is a good solvent for P3HT molecules, whereas, water is non solvent due to its high polar protic nature. THF is completely miscible in water. In the preparation method of polymer nanoparticles, THF solution of P3HT was rapidly injected into de-ionized water under stirring condition and consequently the individual polymer chains were forced to assemble to form polymer nanoparticle (PNPs). On this consequence, Potai et al. demonstrated that the red shifted absorption spectrum of PNPs

was observed due to the increment of effected conjugation length inside PNPs.[36] For further clarification, fluorescence study of P3HT polymer in THF and P3HT PNPs dispersed in water is undertaken. For this purpose, both the samples were excited with 400 nm wavelength of excitation. The PL peak is observed at 560 nm for P3HT in THF and the PL peak at 596 nm is obtained for polymer NPs with lower intensity due to the formation of PNPs, (Figure S2). The relative quantum yield (with respect to rhodamine 6G dye molecules) of P3HT in THF medium is 17.2%, whereas, it becomes 3.4 % after formation of PNPs which supports the coiling of polymer chain upon P3HT PNPs formation.

After attachment of Au NPs on P3HT PNPs, a gradual bathochromic shift and the enhancement of absorption band of P3HT PNPs are due to electronic interactions between the exciton and plasmon (fig 2A). Finally, after addition of Au NPs having a concentration of 7.8 nM, the absorption of P3HT NP is shifted to 459 nm (from 440 nm to 459 nm) (fig 2B). The red shifting as well as spectral broadening of the absorption band occur due to the aggregation phenomena of Au NP on polymer nanoparticle surface (Fig S3).[37] However, no spectral shifting is observed in absence of surface modification by HDA (Fig. S4), indicating Au NPs are interacting strongly with P3HT PNP surface in presence of HDA. It is interesting to note that the extinction coefficient (at 459 nm of wavelength) increases from of 1.75 x 10^6 $dm^3mol^{-1}cm^{-1}$ (pure P3HT PNP) to 2.35 x 10^6 $dm^3mol^{-1}cm^{-1}$ (P3HT/Au composite) which leads to increase visible light absorption. As a result, larger numbers of photo-generated excitons are generated after photoexcitation of this composite system. Thus, Au NPs attached P3HT PNPs hybrid system enhances the charge separation which eventually influences the photo-catalytic properties.

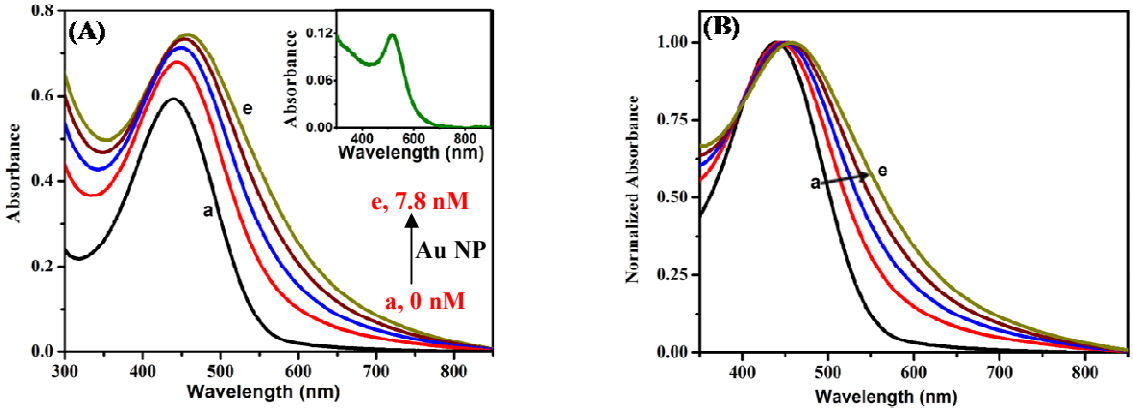

Fig. 2: (A) UV-visible absorption spectra of P3HT PNPs with gradual increase in concentration of 0 nM (a), 3.1 nM (b), 4.7 nM (c), 6.3 nM (d) and 7.8 nM (e) of Au NPs (Inset shows the plasmon band of pure Au NPs at concentration of 7.8 nM). (B) Normalized UV-visible absorption spectra of P3HT PNPs with gradual increase in concentration of 0 nM (a), 3.1 nM (b), 4.7 nM (c), 6.3 nM (d) and 7.8 nM (e) of Au NPs.

It is seen from the Fig. 3 that the PL intensity (excited at 400 nm) of P3HT PNPs (prepared with HDA) is decreased with increasing Au NPs concentration. In control experiment, little change in PL quenching is observed when Au NPs (7.8 nM) solution is mixed with P3HT PNPs without HDA (Fig. S5). It reveals that Au NPs are strongly interacting with P3HT PNPs in presence of HDA because of the close proximity upon attachment of Au NPs with the P3HT PNPs. PL quenching of P3HT PNPs (with HDA) may be ascribed due to the following two reasons: (1) either due to energy transfer from P3HT PNPs to Au NPs and/or (2) due to charge transfer reaction, leads to electron transfer from P3HT PNPs to Au NPs.

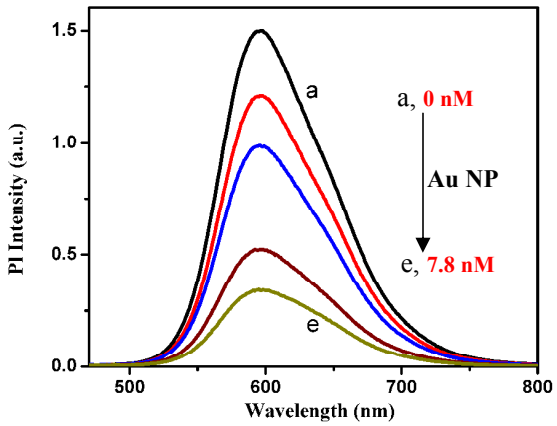

Fig. 3: Photoluminescence spectra of P3HT PNPs with gradual increase in concentration of 0 nM (a), 3.1 nM (b), 4.7 nM (c), 6.3 nM (d) and 7.8 nM (e) of Au NPs at 400 nm excitation.

To understand the PL quenching mechanism, we perform TCSPC measurements where all the samples are excited at 375 nm and decay times of the corresponding samples are measured at 596 nm emission. Fig. 4 depicts the fluorescence decays of P3HT PNPs (surface modified by HDA) in presence of 0 nM and 7.8 nM of Au NPs solution. Average decay time of P3HT PNPs is decreased from 491.6 ps to 257.8 ps with addition of Au NPs. Bi-exponential decay curve with the combination of 366 ps (80%) and 994 ps (20%) is observed for the P3HT PNPs in absence of Au NPs. After the addition of Au NPs, the decay curve is changed to tri-exponential with a combination of 142 ps (76.5%), 596 ps (21.7%) and 1.1 ns (1.8%). It is seen that the decay dynamics is affected predominantly with the faster part over slower part after addition of Au NPs, which imply faster photo induced processes in presence of Au nanoparticles.

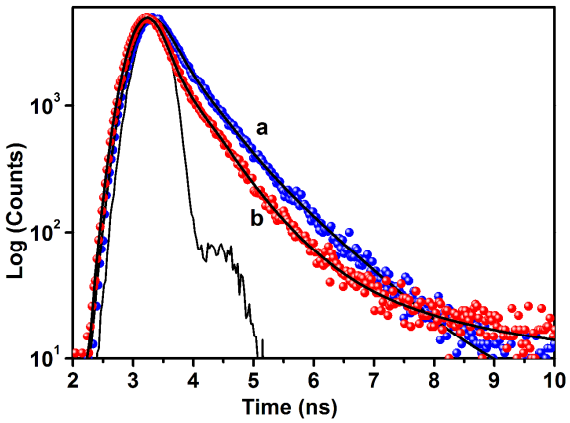

Fig. 4: Time resolved emission decay curves (λ_{ex} 375 nm, λ_{em} 596 nm) of pure P3HT PNPs (a) and with addition of Au NPs (7.8 nM) (b).

For further investigation on shorter time scale, we have performed a femtosecond fluorescence upconversion experiment. In case of femtosecond fluorescence upconversion, the faster part of the decay lifetime is measured. Here, all the samples under investigation were excited at 400 nm and lifetimes were measured at 596 nm emission. It is clear from the fig. 5 that significant changes in ultrafast part are observed in addition of Au NPs. Fitted decay parameters for all the decay curves are given in Table 1. It is clearly seen from Table 1, not only the faster part of the lifetime is decreasing but the corresponding contribution of each lifetime is also increasing with increasing Au NPs from 0 nM to 7.8 nM. The shortening of lifetime may be ascribed due to very faster non-radiative relaxation processes and/or charge transfer process.[38]

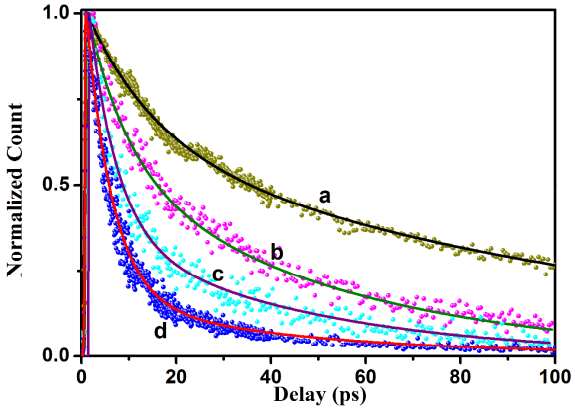

Fig. 5: Femtosecond fluorescence upconversion decays (λ_{ex} 400 nm, λ_{em} 596 nm) of pure P3HT PNPs (a), with increasing the concentration of 3.1 nM (b), 4.7 nM (c), and 7.8 nM (d) of Au NPs.

We have also examined the photo-catalysis properties of P3HT PNPs/Au NPs composite with Au NPs, P3HT PNPs (using 7.8 nM of Au NPs) using methylene blue (MB) dye as probe molecule. The photo-catalysis experiment was carried out under visible light irradiation because P3HT PNPs and P3HT PNPs/Au NPs composite both have a good absorbance in the visible region. Under visible light irradiation, Frenkel type of exciton is generated which is composed of holes in the highest occupied molecular orbital, HOMO (h^+_{HOMO}) and electrons in the lowest unoccupied molecular orbital, LUMO (e^-_{LUMO}) in P3HT PNPs (equation 1) and that is difficult to separate due to their higher binding energy (~0.8-1 eV).[39] In case of P3HT PNPs /Au NPs composite, as Au NPs act as good electron reservoir, photo-generated excitons are decomposed at the interface of the hybrid system and as a result electrons immediately move from LUMO of P3HT to Au NPs (equation 2) to create a separation between electrons and holes (Shown in Scheme 1), causes photoinduced interfacial charge transfer system.[16] The photo generated electrons on the surface of Au NPs then react with dissolved oxygen molecules present in water and yield superoxide radical anions ($O_2^{\bullet -}$) (equation 3), which then react with water to generate hydroperoxy radicals ($OH^{\bullet}$) (equation 4

and 5). The remaining holes present inside the P3HT PNPs may react with water to form hydroperoxy radicals ($OH^{\bullet}$) (equation 6). $OH^{\bullet}$ is a strong oxidising agent and it finally degrades the MB (equation 7). The mechanism of photo-catalysis is given as follow:[40]

$$P3HT + h\nu \rightarrow P3HT (e^-_{LUMO}.....h^+_{HOMO}) \quad (1)$$

$$P3HT (e^-_{LUMO}.....h^+_{HOMO}) + Au\ NPs \rightarrow Au\ NPs (e^-_{LUMO}) + P3HT (h^+_{HOMO}) \quad (2)$$

$$Au\ NPs (e^-_{LUMO}) + O_2 (dissolved\ in\ water) \rightarrow Au\ NPs + O_2^{\bullet -} \quad (3)$$

$$O_2^{\bullet -} + H_2O \rightarrow OH_2^{\bullet} + H_2O_2 \quad (4)$$

$$H_2O_2 \rightarrow 2\ OH^{\bullet} \quad (5)$$

$$P3HT (h^+_{HOMO}) + H_2O \rightarrow OH^{\bullet} + H^+ \quad (6)$$

$$OH^{\bullet} + MB \rightarrow Degraded\ MB + CO_2 + H_2O \quad (7)$$

The degraded product (shown in Equation 7), Leuco-Methylene Blue (LMB) has no absorption in the visible range. To understand proposed mechanism, the formation of $OH^{\bullet}$ is examined by an experiment. In this experiment, terephthalic acid (TA) is used as probe molecule which is excited at 315 nm. For this purpose, same amount of composite (P3HT PNPs / Au NPs) is used with a basic solution of TA instead of MB, (the final concentration of TA is 5×10^{-4} M in an aqueous 2×10^{-3} M concentration of NaOH solution). TA itself is not a fluorescence active compound but at the time of photocatalysis, photo-generated $OH^{\bullet}$ can react with TA to form a highly fluorescent product and the intensity of fluorescence of this product is increased gradually with increasing the time of irradiation of visible light (Fig S6). This suggests that the photocatalysis mechanism is followed through the preparation of $OH^{\bullet}$.

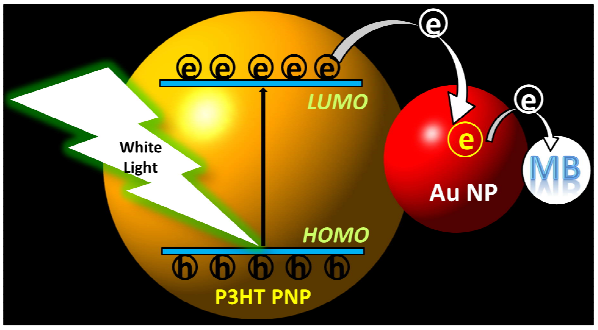

Scheme 1: Schematic representation of photo generated holes and electrons on P3HT PNP and followed by shuttling of electron towards Au NPs and finally degrades MB in a P3HT PNP/Au NP composite system.

Thus, the formation of $OH^{\bullet}$ confirms the occurrence of charge transfer process in our present work. Now, two types of charge transfer processes may happen e.g., (1) electron transfer and (2) hole transfer. In this present research, hole transfer is not possible due to mismatch of HOMO (-3.2 eV) – LUMO (-5.5 eV) band gap of P3HT PNPs with the work function of Au NPs (-5.1 eV). Based on band gap of P3HT PNPs and work function of Au NPs values, electron transfer process can only happen among the charge transfer processes and the electron transfer process occurs from photoexcited P3HT PNPs to Au NPs.

MB has two absorption peaks at 612 nm and 664 nm. At the time of photocatalysis, absorption maximum of MB changes continuously with time of light irradiation due to the production of demethylated MB (depicted in fig 6A). For calculation of catalytic degradation efficiency or catalytic degradation kinetics of MB, we have taken the absorbance value corresponds to 664 nm, which have been widely used elsewhere.[41]

In order to determine the catalytic degradation efficiency (D%), we use the following expression:[40]

$$D\% = \frac{C_0 - C_t}{C_0} \times 100\% \qquad (8)$$

Where C_0 and C_t are the concentrations of MB, respectively before and after the light irradiation at time, t. C/C_0 vs. time plot is given in fig. 6B. The photodegradation reaction of MB follows pseudo-first order reaction dynamics and catalytic degradation rate constant, k (min $^{-1}$) can be written as:[40]

$$\ln\left(\frac{C_0}{C}\right) = kt \quad (9)$$

Figure 6C shows the plot of $\ln\left(\frac{C_0}{C}\right)$ versus time (t) for the photodegradation of MB.

The calculated maximum catalytic degradation efficiencies and the rate constants of the photocatalysis experiment on MB with the different systems are listed in Table 2. After visible light irradiation on MB in the absence of photocatalyst, merely catalytic degradation of the dye is found [Fig 6B (a)]. The maximum catalytic degradation efficiencies are 16.6%, 55% and 90.6% for Au NPs, pure P3HT PNPs and P3HT PNPs /Au NPs composite system, respectively. It is clearly seen that the composite system is 1.6 times higher catalytic degradation efficiency over pure P3HT PNPs. Similar observation is also reflected on the values of rate constants of the photo catalysis reactions. The corresponding rate constants are 1.0 x 10^{-3} min^{-1}, 4.3 x 10^{-3} min^{-1} and 1.29 x 10^{-2} min^{-1} for Au NPs, pure P3HT PNPs and P3HT PNPs /Au NPs composite system respectively. The higher rate constant is found for P3HT PNPs /Au NPs composite system than the pure P3HT PNPs.

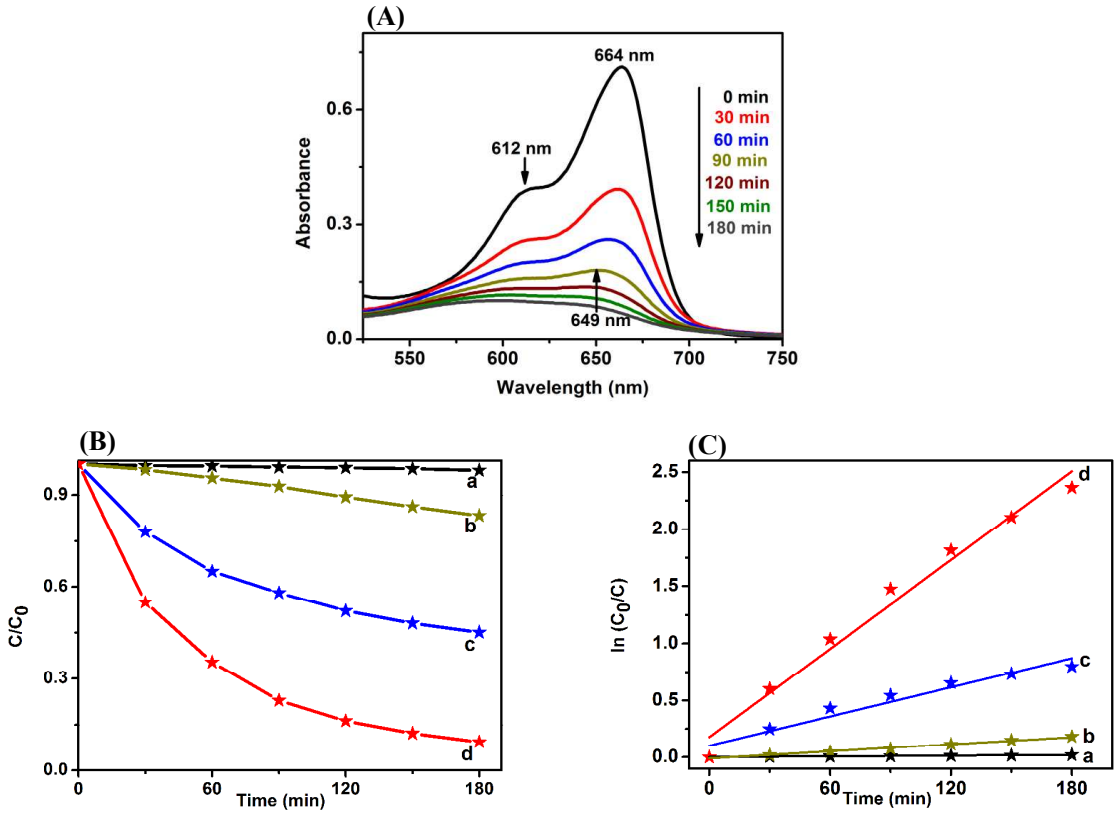

Fig. 6: (A) UV-visible absorption spectra of MB under exposure of visible light irradiation in presence of P3HT PNPs/ Au NPs composite (here 7.8 nM of Au NP is used) (B) Plot of C/ C_0, and (C) Plot of ln(C_0/C) as a function of irradiation time under visible light irradiation of MB containing MB itself (a), Au NP (b), P3HT PNPs (c), and P3HT PNPs/Au NPs composite (d).

Conclusion

In conclusion, raspberry type hybrid nanostructure has been designed through the coulombic interaction between positively charged P3HT PNPs and negatively charged Au NPs by simple solution based synthetic technique. Steady state and time resolved spectroscopy (from picoseconds to femtosecond time resolution) defines the ultrafast photophysical relaxation dynamics of P3HT in presence of surface attached Au NP which is further assigned as charge transfer reaction as well as photo-induced electron transfer process

from P3HT PNPs to Au NPs by photo-catalytic degradation of methylene blue under visible light illumination. The maximum photocatalytic efficiency reaches up to ~91%. To the best of our knowledge, there is no such report where raspberry type organic-inorganic hybrid nanostructure of regio-random P3HT PNPs and Au NPs have been employed as the photocatalyst having >90% photocatalytic efficiency. Analysis reveals that such semiconducting polymer/metal nanoparticle hybrid nanostructures offer exciting opportunities for device technologies.

Experimental Section:

Materials:

Regio-random Poly-3-hexylthiophene (P3HT) (Aldrich), gold (III) chloridetrihydrate ($HAuCl_4$) (Merck), hexadecylamine (HDA) (Aldrich), trisodium citratedihydrate (Merck), methylene blue (MB) (Spectrochem), sodium borohydrate ($NaBH_4$) (Merck), terephthalic acid (TA) (Aldrich), distilled tetrahydrofuran (THF) (Merck), HPLC water (Merck) were used as received for our synthesis in the present study.

Preparation of positively charged P3HT polymer nanoparticles (PNPs):

Aqueous dispersion of positively charged P3HT PNPs is prepared using simple reprecipitation technique described elsewhere.[30-32] First, 300 µL of 1 mg mL^{-1} P3HT in THF, 150 µL of 1 mg mL^{-1} hexadecylamine (HDA) in THF and 150 µL of THF were mixed under inert atmosphere and the mixed solution was ultrasonicated to get a completely homogeneous solution. Then, 500 µL of the mixed solution was rapidly injected into 20 mL of HPLC water under vigorous stirring for 5 min. After a while, this solution was ultrasonicated for 30 min and thereafter the THF was evaporated by partial vacuum evaporation at 60^0C for two hours. Thus, the THF was removed left behind aqueous dispersion of positively charged P3HT PNPs (Fig 1A) which is stable for more than three months.

Synthesis of citrate-capped Au nanoparticles (NPs):

Citrate-capped Au NPs were prepared using a reported method.[33, 34] Briefly, 0.5 mL aqueous solution of $HAuCl_4$ (10mM) and 0.5 mL trisodium citrate (10mM) were added to 19 mL of HPLC water and were vigorously stirred. Then, 0.6 mL of freshly prepared ice cold aqueous solution of $NaBH_4$ (0.1 M) was added to the vigorously stirred solution. The colour of the solution was changed from dark yellow to pink with the formation of Au NPs with an average size of 5.5 ± 0.2 nm (Fig. 1B). The concentration of synthesized Au NPs is 47 nM which is stable for more than one month.

Fabrication of Au nanoparticle on surface modified P3HT NP:

Here, we have started to prepare a set of solutions of P3HT PNPs with different amounts of the solution of Au NPs (Scheme 2). To have this set of solution, 200 µL of the solution of Au NPs was added and amount of the solution of Au NPs was increased with a gradual addition of 100 µL up to 500 µL to the 2.5 mL of P3HT PNPs solution and the final concentration of P3HT PNPs is 317 nM in each 3 mL of total solution. As a result, final concentrations of Au NPs in each 3 mL set of solution are 3.1 nM, 4.7 nM, 6.3 nM and 7.8 nM for 200 µL, 300 µL, 400 µL and 500 µL respectively. The unstable polymer - Au nano-composite is obtained beyond 7.8 nM of Au NPs solution.

Scheme 2: Schematic representation of preparation of P3HT PNPs/ Au NPs composite

Characterization:

Molecular weight of regio-random P3HT was determined by using gel permeation chromatography (GPC) technique. The number average molecular weight (M_n) of the regio-random P3HT polymer were measured by size exclusion chromatography using a Waters 1515 isocratic HPLC pump connected to three Waters Styragel HR1, HR3 and HR4 columns and a Waters 2414 Refractive Index Detector at room temperature (25°C). HPLC grade THF was used as the eluent with a flow rate of 1 mL/min. The number average molecular weight (M_n) of the regio-random P3HT polymer was found to be 32800. A high-resolution transmission electron microscope (HRTEM; JEOL 2010, 200 kV operating voltage) was used to investigate the morphological sizes of Au NPs, P3HT PNPs and P3HT/Au NPs composite. Zeta potential value was measured using a Malveron Zetasizer instrument and all the samples under investigation were dispersed in HPLC water. Room temperature optical absorption spectra were taken by UV-vis spectrophotometer (Shimadzu). Room temperature photoluminescence (PL) studies were carried out by a Fluoromax-P (Horiba JOBIN YVON) photoluminescence spectrophotometer. For the time correlated single photon counting (TCSPC) measurements, the samples were excited at 375 nm using picosecond NANO-LED 370 equipment. The typical full width at half-maximum (fwhm) of the system response using a liquid scatter was about 1.1 ns. The repetition rate was 1 MHz. The fluorescence decays were analysed using IBH DAS6 software. The following equation was used to analyse the experimental time-resolved fluorescence decays,P(t):[42]

$$P(t) = b + \sum_{i}^{n} \alpha_i \exp\left(-\frac{t}{\tau_i}\right) \qquad (10)$$

Here, n is the number of discrete emissive species, b is a baseline correction ("dc" offset), and α_i and τ_i are the pre-exponential factors and excited-state fluorescence lifetimes

associated with the i^{th} component, respectively. For multi-exponential decays the average lifetime, ⟨τ⟩ was calculated from the following equation:

$$\langle \tau \rangle = \sum_{i=1}^{n} a_i \tau_i \quad (11)$$

Where $a_i = \alpha_i / \sum \alpha_i$ and is contribution of the decay component. The quantum yields of P3HT in THF and P3HT PNPs have been measured by using following equation:[42]

$$QY_s = (F_s \times A_r \times \eta_s^2 / F_r \times A_s \times \eta_r^2) \times QY_r \quad (12)$$

Here, 'QY_s' represents the calculated quantum yield of the sample and 'QY_r' represents the standard quantum yield of reference dye rhodamine 6G in ethanol. 'A_r' and 'A_s' represents the actual absorbance value of reference dye and sample, respectively at 405 nm. 'F_s' and 'F_r' define the integrated area of emission spectra excited at 405 nm for samples and reference dye, respectively. 'η' represents the refractive index of the solvent medium.

Ultrafast spectroscopic data were investigated by Femtosecond fluorescence upconversion spectrophotometer using Halcyone ultrafast setup (Coherent). The sample was excited with 400 nm wavelength of excitation, pumped by 800 nm femtosecond (fs) (140 fs pulse width, 80 MHz repetition rate) laser pulse (4.4 W) from a Ti:sapphire oscillator (Chameleon, Coherent) coupled to a second harmonic generator (by BBO type I crystal).The emission wavelength (596 nm) and the gate pulse of the fundamental beam (800 nm) are upconverted by a nonlinear crystal (BBO type II). The FWHM of instrument response function is about 300 fs. The femtosecond time resolved decay data were fitted by Surface Xplorer 2.3 fitting software.

For the photocatalytic measurements, photocatalytic properties of P3HT PNPs and P3HT PNPs/Au NPs composite were measured using the catalytic degradation of MB, a good electron acceptor dye. In this study, 100 µL 2mM MB and 5 mL of prepared P3HT PNPs

were added in HPLC water as such the final volume of the solution was 15 mL, keeping the weight ratio of MB: P3HT was 1: 0.977. For the composite system, same concentration of P3HT PNPs (with a ratio of P3HT PNPs: Au NPs = 5:1) and MB was taken. This solution was then stirred for 2 h in a dark condition. No significant decrease in concentration and the change in spectral pattern of the dye are observed after 2 h in presence of photocatalyst. A 300 W Xe lamp of solar simulator (Newport Corporation) was used as the visible light source. In a dark condition, MB and P3HT PNPs/Au NPs composite are mixed and stirred for 3 h. No change in absorbance of MB is observed. Under illumination of light on the solution of TA in absence of P3HT PNPs/Au NPs composite, no change in fluorescence intensity is observed even after 3h (Fig S7).

Acknowledgement:

"DAE-SRC Outstanding Investigator Award", SERB (DST) and Indo-Spain (DST) are gratefully acknowledged for financial support. BJ thanks CSIR for awarding fellowship and SB thanks IACS for awarding fellowship as RA.

Electronic Supplementary Information (ESI) available:

[Figure S1 and S2 present absorption and emission spectra of P3HT in THF and P3HT PNPs dispersed in water. Fig S3 represents UV-visible absorption spectra of PMMA PNPs, Au NPs (7.8 nM), PMMA PNPs/Au NPs composite and aggregated Au NPs. Figure S4 and S5 depict absorption and emission spectrum of negatively charged P3HT PNPs (without HDA) in absence and presence of Au NPs (7.8 nM) solution. Figure S6 represents the changes in intensity fluorescence spectra of TA measured during the visible light irradiation on P3HT PNPs/ Au NPs composite in a basic solution of TA. Fig S7 represents UV-visible absorption spectra of MB under no illumination in presence of P3HT PNPs/Au NPs composite, plot of C/C_0 vs. time for the photocatalytic degradation of MB under illumination in absence and presence of P3HT PNPs/Au NPs composite and under no illumination in presence of P3HT

PNPs/ Au NPs composite, and changes in intensity fluorescence spectra of TA measured during the visible light irradiation on a basic solution of TA in absence of P3HT PNPs/ Au NPs composite and the corresponding plot of C/C_0 vs. time for fluorescence spectra of TA.]

See DOI: 10.1039/x0xx00000x

Table 1: Femtosecond fluorescence decay parameters and the corresponding rate constants of P3HT PNPs with the addition of Au NPs from 0 μL to 500 μL

Amount of P3HT PNPs (nM)	**Amount of Au NPs (nM)**	**τ_1 (a_1) (ps)**	**τ_2 (a_2) (ps)**	**$< \tau >$ (ps)**
317	0	14.47 (0.32)	110.9 (0.62)	83.55
317	3.1	8.59 (0.44)	49.75 (0.56)	36.89
317	4.7	7.12 (0.72)	45.61 (0.28)	20.61
317	7.8	5.57 (0.84)	42.04 (0.16)	13.13

Table 2: Photocatalytic efficiencies and the corresponding rate constants of different systems

System	**Maximum Photocatalytic Efficiency (%)**	**Rate Constant (min^{-1})**
Au NPs	16.6	1.04×10^{-3}
P3HT PNPs	55.0	4.27×10^{-3}
P3HT PNPs/ Au NPs	90.59	1.29×10^{-2}

References:

1 V. L. Colvin, M. C. Schlamp and A. P. Alivisatos, *Nature*, 1994, **370**, 354-357.

2 N. Tessler, V. Medvedev, M. Kazes, S. Kan and U. Banin, *Science*, 2002, **295**, 1506-1508.

3 G. Jiang, A. S. Susha, A. A. Lutich, F. D. Stefani, J. Feldmann and A. L. Rogach, *ACS Nano*, 2009, **3**, 4127-4131.

4 W. U. Huynh, J. J. Dittmer and A. P. Alivisatos, *Science*, 2002, **295**, 2425-2427.

5 A. P. Wight and M. E. Davis, *Chem. Rev.*, 2002, **102**, 3589-3614.

6 S. Banerjee, S. C. Pillai, P. Falaras, K. E. O'Shea, J. A. Byrne and D. D. Dionysiou, *J. Phys. Chem. Lett.*, 2014, **5**, 2543-2554.

7 S. Bhattacharyya and A. Patra, *J. Photochem. Photobiol. C: Photochem. Rev.*, 2014, **20**, 51-70.

8 G. Chen, J. Seo, C. Yang and P. N. Prasad, *Chem. Soc. Rev*, 2013, **42**, 8304-8338.

9 C. Fan, S. Wang, J. W. Hong, G. C. Bazan, K. W. Plaxco and A. J. Heeger, *Proc. Natl. Acad. Sci. U.S.A.*, 2003, **100**, 6297-6301.

10 J. H. Warner, A. R. Watt, E. Thomsen, N. Heckenberg, P. Meredith and H. Rubinsztein-Dunlop, *J. Phys. Chem. B*, 2005, **109**, 9001-9005.

11 N. C. Greenham, X. Peng and A. P. Alivisatos, *Physical Review B*, 1996, **54**, 17628-17637.

12 M. Y. Odoi, N. I. Hammer, K. Sill, T. Emrick and M. D. Barnes, *J. Am. Chem. Soc.*, 2006, **128**, 3506-3507.

13 M. H. J. Oh, M. Chen, C.-H. Chuang, G. J. Wilson, C. Burda, M. A. Winnik and G. D. Scholes, *J. Phys. Chem. C*, 2013, **117**, 18870-18884.

14 D. S. Ginger and N. C. Greenham, *PRB*, 1999, **59**, 10622-10629.

15 J. Xu, J. Wang, M. Mitchell, P. Mukherjee, M. Jeffries-El, J. W. Petrich and Z. Lin, *J. Am. Chem. Soc.*, 2007, **129**, 12828-12833.

16 C. Giansante, R. Mastria, G. Lerario, L. Moretti, I. Kriegel, F. Scotognella, G. Lanzani, S. Carallo, M. Esposito, M. Biasiucci, A. Rizzo and G. Gigli, *Adv. Funct. Mater.*, 2015, **25**, 111-119.

17 S. Bhattacharyya, T. Sen and A. Patra, *J. Phys. Chem. C*, 2010, **114**, 11787-11795.

18 S. Bhattacharyya, B. Paramanik, S. Kundu and A. Patra, *ChemPhysChem*, 2012, **13**, 4155-4162.

19 A. A. Lutich, G. Jiang, A. S. Susha, A. L. Rogach, F. D. Stefani and J. Feldmann, *Nano Lett.*, 2009, **9**, 2636-2640.

20 C. Sanchez, B. Julian, P. Belleville and M. Popall, *J. Mater. Chem.*, 2005, **15**, 3559-3592.

21 M. Kaltenbrunner, M. S. White, E. D. Głowacki, T. Sekitani, T. Someya, N. S. Sariciftci and S. Bauer, *Nat. Commun.*, 2012, **3**, 770.

22 P. F. Barbara, A. J. Gesquiere, S.-J. Park and Y. J. Lee, *Acc. Chem. Res.*, 2005, **38**, 602-610.

23 B. C. Sih and M. O. Wolf, *Chem. Commun.*, 2005, 3375-3384.

24 M. Achermann, *J. Phys. Chem. Lett.*, 2010, **1**, 2837-2843.

25 G. D. Scholes and G. Rumbles, *Nat. Mater.*, 2006, **5**, 683-696.

26 T. Sen and A. Patra, *J. Phys. Chem. C*, 2012, **116**, 17307-17317.

27 M. A. El-Sayed, *Acc. Chem. Res.*, 2001, **34**, 257-264.

28 D. M. Stevens, Y. Qin, M. A. Hillmyer and C. D. Frisbie, *J. Phys. Chem. C*, 2009, **113**, 11408-11415.

29 H. B. Michaelson, *J. Appl. Phys.*, 1977, **48**, 4729-4733.

30 H. Shimizu, M. Yamada, R. Wada and M. Okabe, *Polym. J*, 2007, **40**, 33-36.

31 S. Bhattacharyya, B. Paramanik and A. Patra, *J. Phys. Chem. C*, 2011, **115**, 20832-20839.

32 S. Bhattacharyya, B. Jana and A. Patra, *ChemPhysChem*, 2015, **16**, 796-804.

33 N. R. Jana, L. Gearheart and C. J. Murphy, *Langmuir*, 2001, **17**, 6782-6786.

34 T. Sen and A. Patra, *J. Phys. Chem. C*, 2008, **112**, 3216-3222.

35 F. Wang, M.-Y. Han, K. Y. Mya, Y. Wang and Y.-H. Lai, *J. Am. Chem. Soc.*, 2005, **127**, 10350-10355.

36 R. Potai and R. Traiphol, *J. Colloid Interface Sci.*, 2013, **403**, 58-66.

37 Y. Kobayashi, Y. Tadaki, D. Nagao and M. Konno, *Journal of Physics: Conference Series*, 2007, **61**, 582.

38 S. Ghosh, S. K. Mondal, K. Sahu and K. Bhattacharyya, *J. Phys. Chem. A*, 2006, **110**, 13139-13144.

39 X.-F. Ren, A.-M. Ren, J.-K. Feng and X. Zhou, *Org. Electron.*, 2010, **11**, 979-989.

40 S. Khanchandani, S. Kundu, A. Patra and A. K. Ganguli, *J. Phys. Chem. C*, 2013, **117**, 5558-5567.

41 J. S. Lee, K. H. You and C. B. Park, *Adv. Mater.*, 2012, **24**, 1084-1088.

42 J. R. Lakowicz, *Kluwer Academic/ Plenum Publishers: New York*, 1999, **3rd ed**, pp 354-464.